3-2011

The Ultrafast Photoisomerizations Of Rhodopsin And Bathorhodopsin Are Modulated By Bond Length Alternation And Hoop Driven Electronic Effects

Igor Schapiro

Mikhail Nikolaevich Ryazantsev

Luis Manuel Frutos

Nicolas Ferre

Roland Lindh

See next page for additional authors

Author(s)
Igor Schapiro, Mikhail Nikolaevich Ryazantsev, Luis Manuel Frutos, Nicolas Ferre, Roland Lindh, and Massimo Olivucci

JACS
JOURNAL OF THE AMERICAN CHEMICAL SOCIETY

ARTICLE

pubs.acs.org/JACS

The Ultrafast Photoisomerizations of Rhodopsin and Bathorhodopsin Are Modulated by Bond Length Alternation and HOOP Driven Electronic Effects

Igor Schapiro,[†] Mikhail Nikolaevich Ryazantsev,[†] Luis Manuel Frutos,[‡] Nicolas Ferré,[§] Roland Lindh,[∥] and Massimo Olivucci*[,†,⊥]

[†]Chemistry Department, Bowling Green State University, Bowling Green, Ohio 43403, United States

[‡]Departamento de Química Física, Universidad de Alcalá, 28871 Alcalá de Henares, Madrid, Spain

[§]Laboratoire Chimie Provence UMR 6264, Université de Provence, Campus Saint Jérôme Case 521, 13397 Marseille Cedex 20, France

[∥]Department of Quantum Chemistry, Ångströmlab, Lägerhyddsv. 1, Box 518, 751 20 Uppsala University, Sweden

[⊥]Dipartimento di Chimica, Università degli Studi di Siena, via Aldo Moro 2, I-53100 Siena, Italy

Supporting Information

ABSTRACT: Rhodopsin (Rh) and bathorhodopsin (bathoRh) quantum-mechanics/molecular-mechanics models based on *ab initio* multiconfigurational wave functions are employed to look at the light induced π-bond breaking and reconstitution occurring during the Rh → bathoRh and bathoRh → Rh isomerizations. More specifically, semiclassical trajectory computations are used to compare the excited (S_1) and ground (S_0) state dynamics characterizing the opposite steps of the Rh/bathoRh photochromic cycle during the first 200 fs following photoexcitation. We show that the information contained in these data provide an unprecedented insight into the sub-picosecond π-bond reconstitution process which is at the basis of the reactivity of the protein embedded 11-*cis* and all-*trans* retinal chromophores. More specifically, the data point to the phase and amplitude of the skeletal bond length alternation stretching mode as the key factor switching the chromophore to a bonding state. It is also confirmed/found that the phase and amplitude of the hydrogen-out-of-plane mode controls the stereochemical outcome of the forward and reverse photoisomerizations.

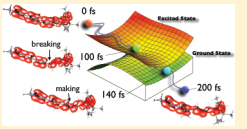

INTRODUCTION

Rhodopsin (Rh) is the G-protein-coupled photoreceptor responsible for twilight vision in vertebrates.[1,2] It comprises an opsin apoprotein and the 11-*cis* retinal protonated Schiff base (PSB11) chromophore covalently linked to the opsin core.[1] The photoexcitation of Rh results in the sub-picosecond isomerization of PSB11 to its *all-trans* isomer (PSBT) that, following picosecond vibrational relaxation, leads to production of the metastable intermediate bathorhodopsin (bathoRh).[3] Low temperature (77 K) irradiation of Rh with 580 nm light establishes, within one second, a photostationary state characterized by a 61:1 Rh/bathoRh ratio showing that bathoRh can be photochemically reconverted to Rh.[4,5] The efficiency of the Rh/bathoRh interconversion is consistent with the fact that these species have close molar extinction coefficients ($4.06 \times 10^4\ M^{-1}\ cm^{-1}$ at 498 nm for Rh and $3.52 \times 10^4\ M^{-1}\ cm^{-1}$ at 535 nm for bathoRh)[4,5] and that the quantum yields for the Rh → bathoRh and bathoRh → Rh photoreactions are 0.67 and 0.49 respectively.[4] Notice that, while bathoRh is stable at cryogenic temperatures, at room temperature it relaxes (via a series of intermediates) to metarhodopsin II, which, in turn, triggers phototransduction by activating the G-protein transducin.[2,6] Therefore the photoisomerization of bathoRh competes with phototransduction. Intensive illumination of Rh also leads to the formation of isorhodopsin,[3] a Rh isomer containing the 9-cis retinal chromophore. However, this reaction is significantly less efficient than the Rh/bathoRh interconversion.[7−9]

Recent computational studies have elucidated the excited state isomerization dynamics of Rh using *ab initio* multiconfigurational quantum chemistry.[10,11] It has been shown that the chromophore reactive π-bond completely breaks on a 100 fs time scale via a bicycle-pedal motion[12−14] that leads to excited state decay. This result has been recently confirmed and experimentally tested by other groups.[15] In spite of its central role in phototransduction, we are unaware of any analogue study carried out for bathoRh. A study of the photoisomerization dynamics of bathoRh appears of basic theoretical interest as the Rh → bathoRh and bathoRh → Rh isomerizations constitute the components of a photochromic cycle/equilibrium implemented at the biological level. In Scheme 1 we outline the simplest mechanism for a photochromic cycle based on two ultrafast (barrierless) π-bond photoisomerizations. The central mechanistic element of the cycle is a conical intersection[16] featuring a fully broken π-bond and mediating excited state decay in both directions. Notice that, at the conical intersection, the *E*/*Z* stereochemical signature is lost. From Scheme 1 it is apparent

Received: June 26, 2010
Published: February 22, 2011

Scheme 1. PSB11 Chromophore Structure and the Elementary (Simplest) Mechanism for Ultrafast Rh/bathoRh Photochromic Interconversion

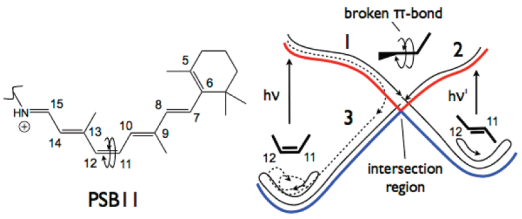

that the simulation of the dynamics of the forward and reverse reaction is expected to (a) provide information on the time-dependent structural and electronic features that make an isomerization successful (trajectory 1 and 2) or aborted (e.g., trajectory 3 for Rh) and (b) unveil the rules that control the stereochemistry of the π-bond reconstitution as trajectories 1 and 2 accomplish this process in opposite directions.

The above target appears of basic importance in the perspective of controlling the Rh/bathoRh isomerization efficiency with tailored excitation light-pulses. By focusing on the related retinal protein bacteriorhodopsin, Prokhorenko, Miller and coworkers[17] have shown that by manipulating the phases and amplitudes of a laser pulse it is possible to enhance or suppress by 20% the quantum efficiency of the retinal chromophore isomerization. The pulses are apparently able to steer the isomerization through constructive and destructive interference effects involving vibrational modes displaced along the reaction coordinate and within the time scale of coherent chemistry (i.e., prior to intermolecular vibrational energy redistribution). As mentioned in ref 18 the shaped pulse must alter the mode amplitude and phase relationship imposed by the potential energy surfaces accessed via photoexcitation. The analysis of these relationships appears of paramount importance if an understanding of the achieved quantum efficiency is needed.

In spite of the fact that previous studies of the dynamics of the production of bathoRh from Rh[15,19,20] and of the isomerization dynamics of isolated or solvated retinal chromophore models[21−25] have appeared in the literature, we are unaware of any reported trajectory computation employing models where the entire chromophore is treated using *ab initio* quantum chemistry and where a full configuration interaction treatment is applied to the entire π-system. In the present work, Rh and bathoRh quantum-mechanics/molecular-mechanics (QM/MM) models based on an *ab initio* multiconfigurational wave functions are employed to look at the light induced π-bond breaking and reconstitution occurring during the Rh → bathoRh and bathoRh → Rh isomerizations. More specifically, QM/MM semiclassical trajectory computations are used to compare the excited (S_1) and ground (S_0) state dynamics characterizing the opposite steps of the Rh/bathoRh photochromic cycle during the first 200 fs following photoexcitation. We show that the information contained in these data provide an unprecedented insight into the sub-picosecond π-bond reconstitution process which is at the basis of the reactivity of the protein embedded PSB11 and PSBT chromophores. In particular, the data point to the phase/amplitude of the skeletal bond length alternation (BLA) stretching mode as the key factor switching the chromophore to a bonding state. It is also confirmed that, once the bonding state is reached, the phase of the hydrogen-out-of-plane (HOOP) mode controls the stereochemical outcome of the forward and reverse photoisomerizations. However, we find that such control can only be effective if the amplitude of such motion is large enough to offset the bonding prompted by the change of the C10−C11−C12−C13 dihedral (see Scheme 1) driving the reaction.

MODELS AND METHODS

QM/MM models based on *ab initio* multiconfigurational second-order perturbation theory have been shown to provide structures and excitation energies consistent with the observed data. For instance, using a CASPT2//CASSCF/6-31G*/AMBER protocol[26,27] we have shown that a suitably constructed Rh model (i) yields a PSB11 conformation consistent with experiment;[28,29] (ii) reproduces the λ^a_{max} change for a small set of modified rhodopsins;[30] (iii) features S_0-S_1 and S_0-S_2 λ^a_{max} values (478 and 327 nm) 3 kcal·mol^{-1} off the experimental values (498 and 340 nm),[3] a computed 14.6 D change in dipole moment that falls within the observed 13−15 D range[31] and an $S_0 \rightarrow S_1$ oscillator strength value (0.8) that compares well with the experimental quantity (1.0).[3] The same protocol has also been successfully used to evaluate the λ^a_{max} of PSB11 in methanol yielding a 2 kcal·mol^{-1} shift from the experimental value.[26]

Our CASPT2//CASSCF/6-31G*/AMBER protocol is fully described in ref 32. The method is based on a hydrogen link atom and electrostatic embedding schemes with the frontier placed at the $C_\delta-C_\varepsilon$ bond of the Lys296 side chain. The active space comprises the full π-system of PSB11 (12 electrons in 12 π-type orbitals). The AMBER charges account for S_0 polarization effects in a mean-field way.[33] The same charges are used for the S_1 computations with no ad hoc dielectric constant added. The models used in the present work are constructed on the basis of the 2.2 Å resolution 1U19 crystal structure[34] of Rh. In order to interpret the bathoRh trajectory data and estimate the reaction/relaxation time scales we also compute the bathoRh CASSCF/AMBER S_1 minimum energy path (MEP) starting from its Franck−Condon (FC) structure. The MEP was obtained in mass-weighted Cartesian coordinates using the method[35] implemented in GAUSSIAN03.[36]

The semiclassical trajectories are computed with an extended version of the scaled-CASSCF//AMBER protocol recently employed to investigate the S_1 dynamics of Rh.[10] The scaling factors used for correcting the gradient/time[10] are 0.795 and 0.663 for Rh and bathoRh respectively. Two-root state average S_1 and S_0 QM/MM force fields are computed using the MOLCAS[37] developer version 7.5 coupled with the Tinker 4.2 molecular mechanics program.[38] The velocity Verlet algorithm[39] and forces obtained from the same QM/MM setup were used to propagate the Newton's equation of motions (see details in the Supporting Information). Once the S_1 and S_0 state potentials approach, a surface hopping algorithm was employed to detect nonadiabatic transitions between the states. We use an algorithm based on the change of the state-averaged wave functions that has been tested for different systems.[40−49] Briefly: at each time step the S_1 configuration state function coefficient vector is compared with the corresponding S_0 vector of the previous time step. A sudden increase in their scalar product indicates that the orthogonality is no longer conserved pointing to a region featuring a large nonadiabatic (i.e., derivative) coupling and hop probability. In practice, we simulate the hop by changing the root selected for gradient calculation when a 0.5 product value is detected. The energy differences resulting from hopping were recovered in terms of kinetic energy by scaling the velocity vector at the hop point. This is a simplified version of conventional trajectory surface hopping (TSH) protocols which refers to trajectory ensembles mimicking nonadiabatic wavepacket dynamics.[50] As anticipated above, here we focus on mechanistic and stereochemical studies based on the analysis of *different types* of single trajectories (see Scheme 1). We do not discuss statistical

dx.doi.org/10.1021/ja1056196 |*J. Am. Chem. Soc.* 2011, 133, 3354–3364

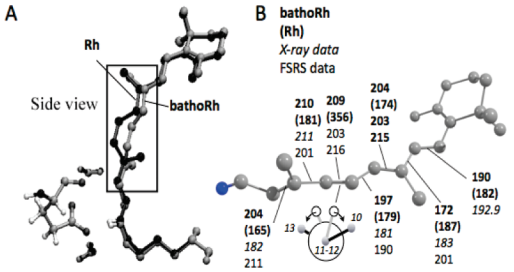

Figure 1. Comparison of Rh and bathoRh S_0 equilibrium structures. A. Superposition of the retinal chromophores. B. Comparison of the relevant computed (in bold) and observed dihedral angles for the bathoRh backbone. The dihedral angles computed for Rh are given in parentheses. All values are in degrees. The Newman projection displays the relative orientation of the C10−C11−C12−C13 backbone segment before (open circles) and after (spheres) the isomerization.

quantities such as quantum yields that would require accurate TSH methods and a statistically significant number of trajectories.[51]

In Figure 1, we show the superposition of the Rh[11] and bathoRh chromophore framework. The major changes are localized in the C9−C10−C11−C12−C13 segment (see Scheme 1) of the backbone. In contrast, the position of the β-ionone ring and that of the protonated Schiff base segment remain substantially unchanged (including the Glu113-chromophore framework). This finding can be rationalized by the fact that the ring is hosted in a tight protein pocket (mainly formed by Thr265, Phe212, and Glu122) and that the acidic hydrogen of the Schiff base is hydrogen-bonded to the counterion. This conclusion is supported both by recent time-resolved Raman measurements demonstrating that the C=N bonds of Rh and bathoRh have substantially the same frequency[52] and by the X-ray data.[53,54] Resonance Raman data indicate that bathoRh has an *all-trans* structure.[55,56] Smith et al.[57] concluded from the solid state ^{13}C-NMR data that the C10−C11 bond is twisted in agreement with this structure. Recent investigations[58,59] refined the ^{13}C-NMR data but did not question the conformation. The circular dichroism spectrum of bathoRh shows a negative peak at 540 nm which is opposite to that of Rh.[60] This was assigned to the change at the C9−C13 portion of the chromophore which agrees with an *all-trans* configuration. The available X-ray crystal structure of bathoRh (PDB ID: 2G87) has a 2.8 Å resolution.[61] This limited resolution makes necessary a computational refinement that, for the chromophore, is quantum mechanical.[62] Recently,[61] the SCC-DFTB, a self-consistent charge density-functional tight-binding method, has been used to refine the chromophore bathoRh crystal structure. In Figure 1 we compare dihedral angles that were reported in refs 63 and 61 to our bathoRh model. The CASPT2//CASSCF/6-31G*/AMBER energy calculation for our bathoRh model gives energy of $S_0 \rightarrow S_1$ 538 nm consistently with the observed value (535 nm).[2]

RESULTS AND DISCUSSION

In Figure 2A we report the CASPT2//CASSCF/6-31G*/AMBER energy profile along the S_1 MEP of bathoRh. This is a barrierless path connecting the FC point to an S_1/S_0 conical intersection ($CI_{bathoRh}$). As shown in Figure 2B the charge transfer character of the S_1 wave function (revealed by a 0.4−0.5 au increase in the charge residing on the β-ionone half of the chromophore) is maintained along the path. The oscillations occurring near $CI_{bathoRh}$ correctly describe the rapidly changing wave function in this region (see also below). The analysis of the reaction coordinate in Figure 2C shows that the initial relaxation (from 0 to 2.6 au) is dominated by a mode describing a backbone bond order inversion (double-bond expansion and single bond

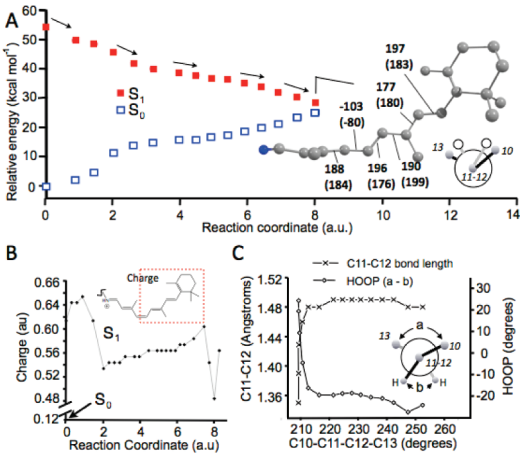

Figure 2. The S_1 MEP of bathoRh. A. Energy profiles along the MEP. Geometrical structures of bathoRh and Rh (in parentheses) conical intersections ($CI_{bathoRh}$ and CI_{Rh} respectively) along the backbone segment of Figure 1A. The values are given in degrees. B. Change in the value of the positive charge fraction residing on the β-ionone containing fragment (framed) along the MEP. C. Analysis of the reaction coordinate in terms of the C11−C12 bond length and HOOP values. The Newman projection provides the definition of the HOOP deformation that is given by the deviation "a − b" of the C10−C11−C12−C13 dihedral angle (indicated as "a") from the H−C11−C12−H value (indicated as "b"). The HOOP value is zero when the C11 and C12 centers are planar.

contraction). However, notice that this is immediately accompanied by HOOP motion at the reactive C11−C12 bond (see legend of Figure 2 for a definition of HOOP). The HOOP value provides a measure of the pyramidalization of the C11 and C12 centers that, in turn, reflects the amount of sp^3 character of the corresponding p-orbitals. As we will see below, this entity is, together with the C10−C11−C12−C13 dihedral change, at the basis of the modulation of the reaction stereochemistry.

After the initial relaxation (beyond 2.6 au) the C10−C11−C12−C13 dihedral describing the backbone isomerization becomes the driving mode (coupled with changes in the C8−C9−C10−C11 and C12−C13−C14−C15 dihedrals). A similar MEP coordinate was reported for Rh.[26] However, after the initial stretching relaxation, the Rh S_1 energy profile becomes flat and shows a tiny energy barrier. The intercepted conical intersection (CI_{Rh}) is less twisted. In a previous report we have provided evidence that intersection structures like CI_{Rh} and $CI_{bathoRh}$ are part of the same S_1/S_0 intersection space.[11]

The QM/MM semiclassical trajectories for bathoRh and Rh were calculated starting at the corresponding FC points on the S_1 energy surface and propagated until unambiguous product identification. The initial velocities are set to zero. It is assumed that the trajectories represent the evolution of the center of the excited state population generated by a laser pulse (i.e., the vibrational wavepacket) and provide a representation of the average dynamics of the systems. This assumption is in line with a recent report[15] that shows that, for Rh, the energy profile and isomerization mechanism associated with a semiclassical trajectory obtained by averaging a set of trajectories defined by different initial conditions (i.e., starting structures and velocities) are close, in terms of energy profile and geometry changes, to those reported in the present work (e.g., compare the Rh energy profiles given below with Figure 6 in the Supporting Information of ref 15. The time predicted for reaching the intersection is also

dx.doi.org/10.1021/ja1056196 |*J. Am. Chem. Soc.* 2011, 133, 3354–3364

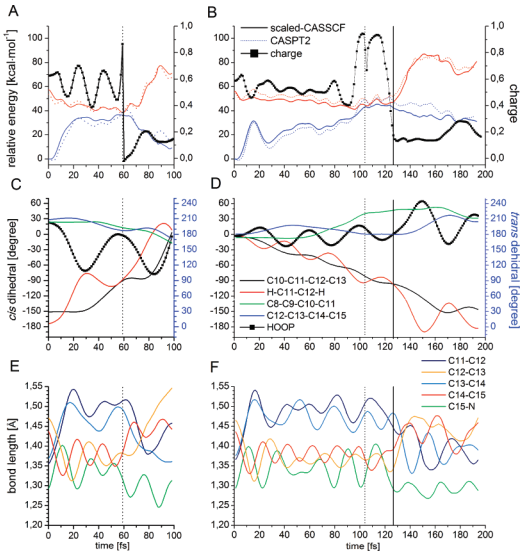

Figure 3. Scaled-CASSCF/Amber trajectories for bathoRh and Rh. A. The S_1 and S_0 energy (left vertical axis) profiles along the trajectory of bathoRh. The change in the fraction of positive charge (right vertical axis) residing on the β-ionone containing fragment is consistent with a sudden change in the electronic structure of the chromophore. B. The same data for Rh. C. Evolution of the main twisting angles and HOOP mode for the bathoRh chromophore. D. The same data for Rh. E. The change in the bond length along the −N−C15−C14−C13−C12−C11 fragment of bathoRh. F. The same data for Rh. The vertical dashed lines at 60 fs (in parts A, C and E) and 104 fs (in parts B, D and F) indicate the hop time. The vertical solid line in parts B, D and F indicates the change of the wave function character along the trajectory.

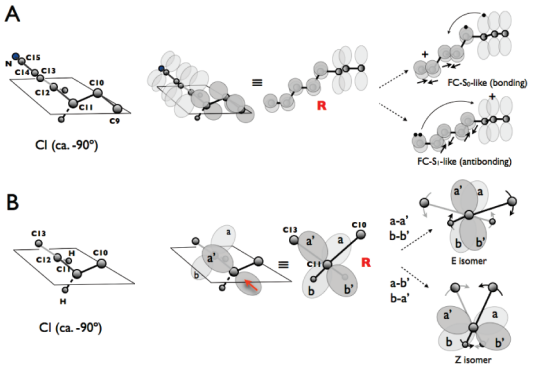

Figure 4. Conditions for C11−C12 π-bond reconstruction in Rh and bathoRh. A. Relationship between the "bond alternation" stretching mode of the N−C15−C14−C13−C12 moiety and the electronic structure of the fully twisted reference structure **R**. The shortening of the N−C15 and C14−C13 bonds stabilizes a diradical structure that correlates with the S_0 state at the chromophore FC point. The expansion of the same two bonds (and compression of the C15−C14 and C13−C12 bonds) leads to a closed-shell configuration that correlates with the S_1 state at the FC point. The curly arrow indicates the electron transfer process transforming one electronic configuration into the other. B. Evolution of the overlap between the π-orbitals at C11 and C12 from **R**. The Newman projection of **R** shows a situation in which the HOOP is zero (i.e., the C10−C11−C12−C13 and H−C11−C12−H dihedral are both ca. −90°) and the C11 and C12 centers are planar sp^2 hybrids. Clockwise and counterclockwise twisting induces equivalent overlaps prompting the formation of the *E* (overlap between lobes a and a′/b and b′) or *Z* (overlap between lobes b and a′/a and b′) isomer respectively.

similar when the scaling required to correct for the different slopes of the CASPT2 and CASSCF energies is applied[10]). This has also been seen when comparing, at the same QM/MM level, the S_1 trajectory of Rh with a series of trajectories starting at torsionally distorted FC points.[10] Given the short (less than 200 fs) time scale simulated in this work, we kept the opsin backbone and side chains fixed at their crystal structure that is assumed to provide a representation of the average opsin environment. The chromophore-Lys296 side chain and the internal waters are left free to evolve during the simulation, for a total of 198 vibrational degrees of freedom.

We find that both trajectories are reactive and generate the photoproduct within the simulation time. The S_1 and S_0 energies computed along the bathoRh and Rh trajectories are reported in Figure 3A and 3B respectively. For bathoRh the S_1-S_0 gap is found to decrease by ca. 40 kcal·mol^{-1} during the first 15 fs. As previously reported[26,64−69] and consistently with the MEP in Figure 2C, the initial relaxation is dominated by bond order inversion along the chromophore backbone. During this time the C10−C11−C12−C13 dihedral angle describing the isomerization remains substantially constant (see Figure 3C). In contrast, the H−C11−C12−H dihedral undergoes a significant +60° change indicating a large (−60°) HOOP motion that leads to large pyramidalization at C11 and C12. This is consistent with a prompt acceleration of the hydrogen atoms at C11 and C12 along a direction that decreases the orbital overlap (and conjugation) across the C11−C12 bond. This process is coupled with the elongation of the C11−C12 bond from 1.36 to 1.54 Å that becomes, effectively, a single bond. The data in Figure 3C and Figure 3D for bathoRh and Rh respectively (see also below) show that the H−C11−C12−H dihedral change (and therefore the HOOP change) is activated 5 fs after photoexcitation. This is faster than the C10−C11−C12−C13 dihedral describing the isomerization which starts moving 15 fs later. Such a fast motion displaces the hydrogens in position C11 and C12 off the double bond plane and leads to sp^3 hybridization. In bathoRh the hydrogens are displaced on the same side of the double bond plane, while in Rh these move in opposite directions. This is consistent with both early resonance Raman[55] and recent femtosecond Raman spectroscopy[63] studies where the Rh → bathoRh dynamics has been studied by following the HOOP changes. During the entire bathoRh trajectory the HOOP and H−C11−C12−H dihedral motion oscillate out-of-phase (see Figure 3C). The amplitude of these oscillations is much larger than in the oscillations of the C10−C11−C12−C13 dihedral that are in-phase with the HOOP mode.

Before describing the S_1 decay and the reconstitution of the broken C11−C12 π-bond, we discuss the stereoelectronic factors involved in such basic processes. The discussion is largely based on the seminal analysis of the ground and excited state electronic structure of protonated Schiff bases reported by Michl and Bonačić-Koutecký.[70,71] As illustrated in Figure 4, the formation of a π-bond along a conjugated chain occurs when two conditions are met: (i) the wave function allows for electron pairing (a bonding state) between the two centers of the conjugated moieties forming the π-bond and (ii) the overlap of the fragment π-orbitals spanning the two conjugated moieties forming the π-bond is not zero.

Condition i is met when the electronic structure of the chromophore is dominated by a resonance structure (the FC-S_0-like, diradical structure of Figure 4A) displaying the positive charge on the −NH═CH− fragment as found for the S_0 state of

dx.doi.org/10.1021/ja1056196 |*J. Am. Chem. Soc.* 2011, 133, 3354–3364

bathoRh (see Figure 2B) where the ca. 88% of the positive charge is placed on the −N−C15−C14−C13−C12− moiety. The condition is not met when the electronic structure is dominated by a charge transfer configuration (the FC-S_1-like, charge transfer structure of Figure 4A). This is the case of the S_1 state of the bathoRh chromophore where 66% of the positive charge is placed on the −C7−C8−C9−C10−C11− moiety. (Notice that near the conical intersection this charge translocation reaches values above 0.9. This is a manifestation of the "sudden polarization effect"[73,74] that, consistently with early results, occurs when the system is approaching the conical intersection and that has a lifetime limited to tens of femtoseconds. See also Figure 3B for Rh.) As a consequence, in a situation where the C11−C12 bond is fully twisted (i.e., as in the reference structure **R**), a change in the bond length alternation (BLA) of the −N−C15−C14−C13−C12− moiety can control the electronic structure of the fragment and thus its bonding or antibonding status (see Figure 4A). Such status determines if, upon S_1 decay, the system will immediately form a double bond or if it will relax along S_0 in the form of a transient charge transfer species. This will eventually change its electronic structure before a photoproduct is generated.

Condition ii controls the stereochemistry of the decay to S_0. As illustrated in Figure 4B, this condition can be met when one of two stereoelectronic requirements is satisfied. In the figure the reference structure (**R**) has near zero overlap between the fragment π-orbitals (represented by the p-orbitals at C11 and C12). Twisting about the C11−C12 bond in a clockwise or counterclockwise direction induces π-bond formation in stereochemically distinct configurations (*E* or *Z*) and independently on the stereochemistry of the reactant π-bond. Such process is at the core of the reaction efficiency in the sense that bond reconstitution leading to the original chromophore stereoisomer (e.g., *Z* for Rh and *E* for bathoRh) will result in a decreased quantum yield (and increased internal conversion).

As shown in Figure 3A, bathoRh enters the S_1/S_0 intersection space ca. 60 fs after photoexcitation when a surface-hop occurs delivering the system to S_0. As reflected by the sudden change in the charge distribution along the chromophore backbone (from ca. 0.9 to less than 0.1, see Figure 3A), the hop is accompanied by the switching of the electronic structure from an antibonding to a bonding state. According to the diagram of Figure 4A this change can be induced by specific displacements of the BLA mode. Indeed, as shown in Figure 3E, at the decay point one has a small and/or decreasing values for the N−C15 and C14−C13 bonds and larger and expanding values for the C15−C14 bond. This kind of progression biases the electronic structure toward a region of the S_0 energy surface characterized by radical states for the two moieties of the twisted chromophore and, in turn, leading to facile C11−C12 π-bond reconstitution (via recoupling of the radical centers).

An important stereoelectronic event seems to occur during the first 20 fs following S_1 decay. While during this time the C10−C11−C12−C13 torsional deformation remains substantially constant at a ca. −85°, the H−C11−C12−H dihedral changes rapidly going from a −90° to −30° value. As a consequence the C11 and C12 center becomes highly pyramidal, yielding a −80° value for the HOOP mode. In Figure 5 we report a schematic representation of this process and show how the hybridization of the p-orbitals at C11 and C12 can control the stereochemistry (*Z* or *E*) of the reconstituting π-bond. Starting from the reference structure **R** (already seen in Figure 4 and representing the decay

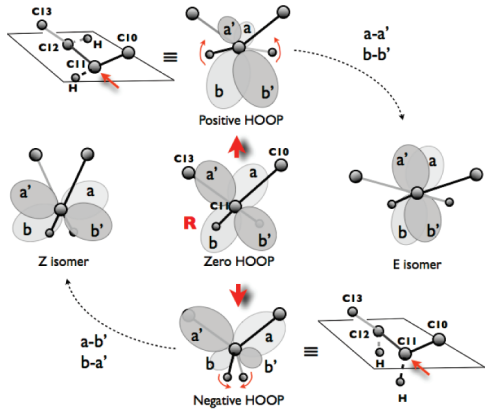

Figure 5. Effect of the HOOP (and H−C11−C12−H dihedral) on the double-bond photoisomerization stereoselectivity. **R** refers to a situation in which the HOOP is zero (i.e., the C10−C11−C12−C13 and H−C11−C12−H dihedrals are both ca. −90°) and the C10−C11−C12−C13 dihedral is slowly changing with respect to the HOOP mode. At **R** the overlap of the p-orbitals at C11 and C12 centers is close to zero. The vibrational deformation toward positive HOOP and negative HOOP values (opening and closing of the H−C11−C12−H dihedral) increases the orbital overlap and prompts the formation of the *Z* or *E* isomer respectively. Positive and increasing HOOP prompts, exclusively, formation of the *E* isomer (large b−b′ and a−a′ overlap) while negative and decreasing HOOP prompts formation of the *Z* isomer (large b′−a and b−a′ overlap). Notice that the illustrated HOOP-sign rules invert for mirror-image configurations featuring positive rather than negative C10−C11−C12−C13 and H−C11−C12−H (angles "a" and "b" in Figure 2C) dihedrals. These rules are related and extend those[46,72] derived through the analysis of a set of trajectories computed for model chromophores.

point) the decrease of the HOOP value leads to opposite sp^3 hybridizations at C11, C12 and, in turn, to an increase in overlap between the p-orbitals at these centers. The negative HOOP value results into a displacement prompting the formation of a π-bond with an 11-*cis* stereochemistry (in Figure 5 lobe "a" interacts with lobe "b′" while lobe "a′" interacts with lobe "b"). This conclusion is strongly supported by the π-electron density analysis reported in Figure 6A which indicates that the value of the HOOP mode immediately after the wave function change (independently on when this change is occurring: at the same time of the decay or later) is critical for efficient photoproduct formation. Again, notice that this conclusion and the HOOP rules are valid when the local amplitude of the HOOP change is larger than the change in the C10−C11−C12−C13 dihedral angle driving the isomerization. This point will be further discussed at the end of the present section.

According to our trajectory, the photolysis of bathoRh leads to an extremely distorted form of the 11-*cis* π-bond of the Rh chromophore already 80 fs after photoexcitation to S_1 and 20 fs after the decay to S_0. During the following 20 fs the trajectory describes a planarization of the C11−C12 bond that is completed on a 100 fs time scale (see Figure 3C). Notice that, at this point, the retinal chromophore does not have the structure of the equilibrated PSB11 yet. The computed excitation energies during the last 10 fs of the trajectory (between 90 and 100 fs; see Figure 3A) correspond to an absorption between 540 and 610 nm and are thererefore considerably red-shifted with respect to our relaxed Rh model (478 nm).

The 100 fs bathoRh isomerization described above takes place in the confined space of the protein binding pocket and must thus

dx.doi.org/10.1021/ja1056196 |*J. Am. Chem. Soc.* 2011, 133, 3354–3364

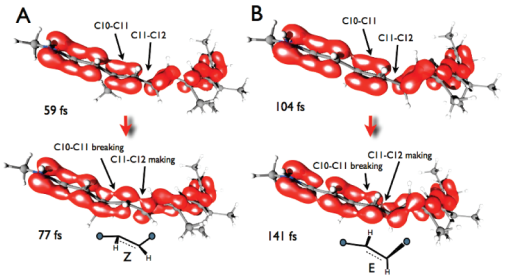

Figure 6. Two snapshots of the S_0 π-electron density along the semiclassical trajectories of Figure 3. A. bathoRh to Rh trajectory (see the movie in the Supporting Information for the complete evolution). B. Rh to bathoRh trajectory (see the movie in the Supporting Information for the complete evolution). The π-electron density snapshots at the top are taken at the surface hop (59 and 104 fs). The similarity of these structures is consistent with the fact that the corresponding conical intersection structures belong to a common intersection space.[11] The π-electron density snapshots at the bottom give points where the C11−C12 double bond reconstitution is visualized by plotting the electron density with an isodensity value of 0.27. In both cases the comparison between the top and bottom density plots shows that the bond formation process has begun with a stereochemistry leading to PSB11 (Z) or PSBT (E) for bathoRh and Rh respectively.

adopt a space-saving reaction coordinate. Consistently with the computed S_1 MEP, the bathoRh trajectory shows that the clockwise twisting around the C11−C12 reactive bond is accompanied by partial 30°−40° counterclockwise twists of the adjacent C9−C10 and C13−C14 bonds (see Figure 3C). These twists are required to accomplish the isomerization without significant displacement of the β-ionone ring and of the Schiff-base moiety bounded to Lys296 and allow the isomerization in the confined opsin space. We also find that such motion is substantially reversed with respect to the previously reported[10] bicycle-pedal motion driving the photoisomerization of Rh (see below).

The energy profiles along the semiclassical trajectories of Rh (Figure 3B) have features in common with those of bathoRh (Figure 3A). For instance the S_1-S_0 energy gap falls by more than 50 kcal·mol^{-1} in the first 15 fs. The cause of this evolution is the inversion of the bond length alternation which takes place in the same time frame. In addition, similar to bathoRh, the changes in the H−C11−C12−H dihedral (see Figure 3D) are much earlier than the changes in the C10−C11−C12−C13 dihedral. However, in Rh the S_1 decay event is achieved on a slower, 100 fs, time scale. Accordingly, notice that before decay the Rh chromophore performs three complete HOOP oscillations with amplitudes significantly smaller than in bathoRh.

The largest differences between bathoRh and Rh are seen after the decay and during S_0 relaxation. After the decay the Rh trajectory evolves (for ca. 20 fs) through a region where the S_0 and S_1 states are close in energy. In this region the S_0 wave function is dominated by an antibonding character (see the positive charge evolution in Figure 3B) and thus the π-bond does not reconstitute. This region of the Rh potential energy surface has been discussed in ref 75, which reports on the shape of the S_0 and S_1 potential energy surfaces in the vicinity of a −90° twisted conical intersection CI (i.e., close to $CI_{bathoRh}$ and CI_{Rh}). The results are summarized in Figure 7A by displaying the CASPT2//CASSCF energy profile along a loop centered on the intersection point.

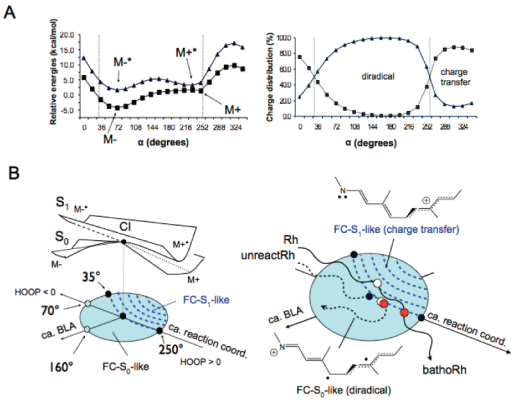

Figure 7. Structure of the conical intersection of Rh. A. S_0 (squares) and S_1 (triangles) energy profiles (left) and charge distributions on the β-ionone containing half of the chromophore (right) along a small loop centered on a conical intersection and lying on the branching plane described in refs 30 and 75. B. Schematic representation of the structure of the S_0 and S_1 potential energy surfaces surrounding the conical intersection (CI). The circle corresponds to the branching plane loop of part A. The vectors corresponding to the branching plane coordinates are molecular modes dominated by a single-bond/double-bond length alternation (BLA) stretching mode and to a complex mode containing components of the HOOP and isomerization coordinates.[75] This last mode is assumed to represent the local reaction coordinate. The BLA mode changes the S_0 electronic structure effectively. The top and bottom structures on the right represent, in terms of resonance formula, the FC-S_1-like (top) and FC-S_0-like (bottom) electronic structures dominating the different regions of the area of the S_0 potential energy surface defined by the circle.

Before reporting on the evolution of Rh after the decay to S_0, we need to revise the main results of ref 75. It is shown that, along a small loop centered on the CI point and lying on the plane defined by the branching plane vectors (that correspond, roughly, to the BLA mode and isomerization mode), one locates two entry (M+* and M−*) and two exit (M+ and M−) channels. These are defined by the minima of the S_1 and S_0 energy profiles along the loop (see Figure 7A left). The two exit channels are oriented at ca. 180° with respect to each other (i.e., in opposite direction with respect to the CI) and describe displacements leading toward Rh and bathoRh respectively.[75] The two entry channels are located almost above the exit channels and support a shape of the S_1 and S_0 energy surfaces consistent with that reported in Figure 7B left. The exit channel (M−) leading to Rh is entered after progression along an S_1 entry channel (M+*) driving bathoRh relaxation and featuring a small S_1-S_0 energy gap. This is consistent with the terminal part of the MEP energy profiles of Figure 2A and of the trajectory energy profiles of Figure 3A (<10 kcal mol^{-1} S_1-S_0 gap). It has also been reported[75] that along the loop the wave function changes twice by passing from an S_0-like diradical character to an S_1-like charge transfer character (see Figure 7A right). The change in wave function along the loop defines two S_0 potential energy regions surrounding the conical intersection that are characterized by different electronic structures. These regions are schematically visualized on the coordinate plane of Figure 7B where the region dominated by the FC-S_1-like (antibonding) character is marked by a dashed area. The change in the nature of the wave function is such that the exit channel driving the system toward Rh is dominated by a bonding (FC-S_0-like) character. In contrast, the exit channel pointing to bathoRh has a mixed

dx.doi.org/10.1021/ja1056196 |J. Am. Chem. Soc. 2011, 133, 3354–3364

FC-S_1-like/FC-S_0-like character. The results in Figure 7A (i.e. in ref 75) appear to be consistent with the energy profiles and changing charge distribution reported in Figure 3A and 3B for bathoRh and Rh respectively. In fact, according to Figure 3A, the S_1 and S_0 energy profiles of bathoRh rapidly separate immediately after the decay to S_0 and the system displays a bonding character leading to rapid C11−C12 π-bond reconstitution. In contrast, the Rh data (see Figure 3B) shows that after the decay the S_1 and S_0 energy profiles remain very close and the electronic structure conserves an FC-S_1-like character.

In Figure 3B we see that during the first 20 fs following the decay of S_1 Rh the C10−C11−C12−C13 dihedral changes from −80° to −90°. However, the analysis of the electron density during this time shows that the reconstitution of the C11−C12 double bond has not started yet. As anticipated above, this is explained by the fact that along this part of S_0 trajectory/energy surface the charge-transfer character of the wave function does not allow for C11−C12 π-bond reconstitution. Indeed, no π-electron density has developed along the C11−C12 bond that remains unbonded (e.g., see the 104 fs structure of Figure 6B). Finally, 130 fs after photoexcitation the system exits the near degeneracy region and within 10 fs displays the typical S_0 charge distribution (see the solid line in Figure 3B) that is maintained for the rest of the trajectory. This process corresponds to the evolution from the point of decay (open circle at ca. 100 fs) occurring within the dashed region of the coordinate plane of Figure 7B to the point in which the dashed region is abandoned (full circle at ca. 130 fs) and a bonding state is achieved. A vibrationally excited form of bathoRh is achieved in 200 fs and features a chromophore with a distorted *all-trans* stereochemistry. It features an S_1-S_0 energy gap corresponding to a 670 and 710 nm absorption and an S_2-S_0 between 450 and 530 nm absorption. The S_1-S_0 absorption is red-shifted with respect to the 538 nm found for our bathoRh model. Therefore, there is the possibility that further cooling occurring after our 200 fs trajectory would generate a ca. 600 nm absorption closer to that of the photoRh intermediate reported in the literature.[2]

As shown in Figure 6B the *E*/*Z* stereochemical decision is achieved in the 140 fs time scale when one clearly see a buildup of the π-electron density between the C11 and C12 centers. At this point in time and in contrast to bathoRh, the phase of the HOOP mode is such that the HOOP is increasing rapidly and reaches positive values (i.e., the absolute value of the H−C11−C12−H dihedral is larger than the C11−C12−C13−C14 dihedral that is ca. −90° and almost constant between 110 and 130 fs time segment). According to the diagram in Figure 5 such a situation prompts a large overlap between lobes "b" and "b′". This overlap drives the π-bond reconstitution that, as a consequence of the positive HOOP value, displays an *all-trans* stereochemistry. Notice that the 20 fs evolution occurring immediately after the decay corresponds to a half HOOP period during which the chromophore maintains an antibonding wave function (see Figure 4A). This lack of reactivity is maintained long enough to set the HOOP to positive values thus allowing the system to achieve the photoproduct *E* stereochemistry when a full FC-S_0-like character is reached.

In order to provide further computational evidence supporting the electronic effects described above, we have constructed a different Rh model (unreactRh) that does not complete the isomerization. The analysis of the trajectory of the reactive Rh model investigated above shows that

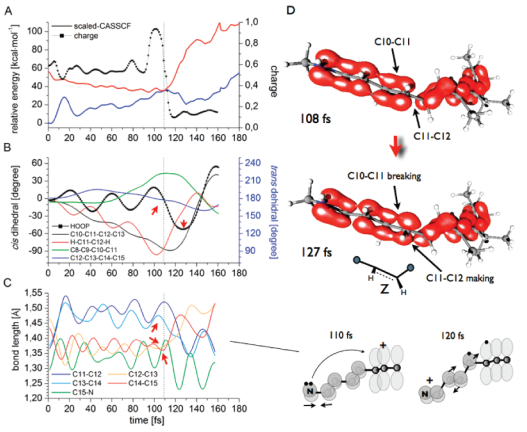

Figure 8. Scaled-CASSCF/Amber trajectory for unreactRh and corresponding evolution of the S_0 π-electron density. A. The S_1 and S_0 energy profiles along the trajectory. The positive charge of the β-ionone containing fragment displays a sudden change in the electronic structure of the chromophore. B. Evolution of the main twisting angles and HOOP mode. The arrows point to the HOOP slope at decay and at the point of the isomerization inversion. C. The change in the bond length along the −N−C15−C14−C13−C12−C11 fragment. The orbital diagrams describe the change in electronic structure completed in 10 fs. The arrows point to the slope of the critical bond lengths at decay. In all parts (parts A, B and C) the vertical dashed line indicates the decay (hop) time. D. The S_1 and S_0 decay (hop) point is detected at 108 fs (see the movie in the Supporting Information for the complete evolution). The comparison between the top and bottom density plots shows that the bond formation process had already begun 20 fs after the decay and leads to a PSB11 (*Z*) stereochemistry.

the $H_{link}-C_\delta-NH-C15-C14-C13-$ chromophore fragment (incorporating the hydrogen link atom) is displaced toward the counterion upon twisting of the reactive C11−C12 bond. The unreactRh model features a spatially fixed H_{link} atom (and a mobile counterion side chain) that restrains the fragment displacement ultimately inducing quantitative changes in the BLA mode phase. In Figure 8 we display the computed 160 fs semiclassical trajectory of unreactRh. Comparison of the Rh and unreactRh trajectory data in Figures 3B, 3D, 8A, and 8B shows that the energy profiles and twisting of the chromophore backbone on S_1 are substantially the same for both systems. In particular, as displayed in Figures 3D and 8B this is true for the oscillatory motion of the HOOP mode and for the progression of the C10−C11−C12−C13 dihedral. However, in contrast to Rh but similar to bathoRh (see Figures 3B and 3A respectively), unreactRh changes electronic structure immediately after decay to S_0 (see Figure 8A) and consequently initiates the C11−C12 π-bond reconstitution immediately after the hop and not after a 20 fs delay (see Figure 3B).

The differences between the Rh and unreactRh trajectories are schematically illustrated in Figure 7B (right). From inspection of Figure 8C, it is apparent that, at the hop, the lengths of the N−C15 and C14−C13 bonds of unreactRh have reached a maximum or are contracting while the C15−C14 bond length has reached a minimum and it is ready to re-expand. This situation rapidly (within 5 fs) leads to a bonding (diradical) character of the wave function consistently with the change in charge distribution displayed in Figure 8A. In Rh the situation is exactly opposite. As displayed in Figure 3F the C15−C14 is contracting and the N−C15 and C14−C13 are expanding biasing the

dx.doi.org/10.1021/ja1056196 |*J. Am. Chem. Soc.* 2011, 133, 3354–3364

electronic structure toward a charge transfer state. The HOOP mode in unreactRh performs slightly more than two and a half oscillations before decay to S_0. At this point the C10−C11−C12−C13 dihedral has a ca. −90° value, while the HOOP mode is decreasing and points to negative values. According to the general rule established above such a situation would lead to formation of the *Z* stereoisomer. Indeed, the trajectory displays a fast change in the C10−C11−C12−C13 dihedral that reverts its direction from counterclockwise to clockwise 120 fs after photoexcitation. In conclusion, the unreactRh trajectory shows that a change in the phase of the HOOP mode during the antibonding to bonding electronic structure change results into an aborted isomerization.

The results above indicate that the HOOP phase modulates the isomerization stereochemistry of trajectories released from their FC points via the orbital overlap rules of Figure 5. However, as stressed above, such rules appear to hold when the ca. 90° twisted C10−C11−C12−C13 dihedral is changing slowly with respect to the HOOP mode. This situation is indeed found in Figures 3C, 3D and 8B. In the following we look at four selected semiclassical trajectories of Rh that start from structures displaced from the FC point. These provide cases where the orbital overlap is determined by competing C10−C11−C12−C13 and H−C11−C12−H (i.e., HOOP) changes.

To obtain realistic initial structures, the configurations of the side chains located within 4 Å from any chromophore atom are sampled via classical molecular dynamics in the presence of a parametrized but geometrically constrained chromophore. The sampling is then continued for both the side chains and the chromophore at the QM/MM level. In practice, four snapshots from the second half of a 2 ns molecular dynamics run are used as starting points for four corresponding 200 fs CASSCF/AMBER (the 3-21G basis set is used to reduce the computational cost) trajectories. The final (i.e., 200 fs) time-steps provide the four initial structures. These are all characterized by limited displacements of the $-C_\delta-N-C15-C14-C13-C12-$ segment and Glu113 (see Figure 9 top). A closer look reveals small and distributed changes in the dihedral angles while the most prominent changes occur in the bond length pattern of N−C15−C14−C13 moiety with differences up to 0.06 Å (in N−C15 bond). An analysis of the relationship between the initial geometrical deformation and the S_1 structural evolution goes beyond the scope of this work. Indeed, here we focus on the impact of the C10−C11−C12−C13, BLA and HOOP changes in the hop region (irrespective of their origin) on the reaction stereochemistry to establish general rules.

It is apparent from inspection of Figure 9A that, when a bonding status is reached (see the vertical full line), the HOOP value is increasing and the C10−C11−C12−C13 dihedral is decreasing. Consistently with the rules of Figure 5, both modes prompt formation of the *E* isomer and the stereochemical outcome is not unambiguous. In Figures 9B and 9C we present increasingly competing situations. In Figure 9B the HOOP is flat (as consequence of the fact that the H−C11−C12−H and C10−C11−C12−C13 dihedrals are changing with the same speed). In this situation the stereochemical outcome is determined by the C10−C11−C12−C13 dihedral motion that points to the *E* isomer. In contrast, in Figure 9C the HOOP moves toward negative values and prompts the formation of the *Z* isomer while the C10−C11−C12−C13 dihedral change points to the *E* isomer. This situation is consistent with the overlap diagram I

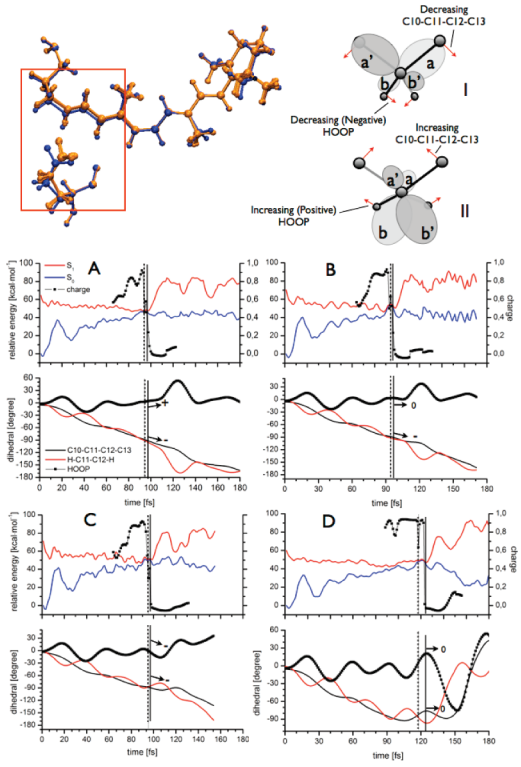

Figure 9. Scaled-CASSCF/3-21G/AMBER trajectories for Rh. Top. Left. A view of the superposition of the FC structure (dark blue) and the four sampled structures discussed in the text. The framed part corresponds to the $-C_\delta-N-C15-C14-C13-C12-$ segment. Right. Competing effects of the changes in the HOOP mode and C10−C11−C12−C13 dihedral. In diagram I the HOOP mode prompts isomerization toward the *E* form while the C10−C11−C12−C13 dihedral prompts isomerization toward the *Z* form. In diagram II the situation is reversed. Panels A−D. Top. The S_1 and S_0 energy (left vertical axis) profiles along the trajectory. The change in the fraction of the charge (right vertical axis) residing on the β-ionone containing fragment is given in the region of the hop from the S_1 to the S_0 state. Bottom. Evolution of the relevant twisting angles and HOOP mode. In all cases the vertical dashed lines indicate the hop time. The vertical solid line indicates the change of the wave function character.

in Figure 9. The decreasing C10−C11−C12−C13 dihedral is increasing the overlap of lobe b with lobe b′ and of lobe a with lobe a′ thus pointing to the *E* configuration. In contrast the increase in the HOOP value (and therefore the increased sp^3 character at C11 and C12) increases the overlap between lobe b with lobe a′ and of lobe b′ with lobe a leading to the *Z* configuration. (Diagram II reports the opposite situation that may apply to bathoRh.) The stereochemical outcome is likely to be determined by the fastest changing overlap and therefore by the fastest changing mode. In Figure 9C we see that after an initial ca. 10 fs inversion in the direction of the C10−C11−C12−C13 change the dihedral continues its evolution toward the photoproduct. Comparison of Figure 9B and 9C leads to the conclusion that an increased HOOP change at the moment of the wave function change will prompt the isomerization to the original *Z* isomer yielding a nonreactive trajectory. This is indeed the case for the unreactRh trajectory seen in Figure 8 in which the HOOP mode is changing more rapidly thus effectively inverting the direction of the C10−C11−C12−C13 change.

dx.doi.org/10.1021/ja1056196 |*J. Am. Chem. Soc.* 2011, 133, 3354–3364

In Figure 9D we present a situation similar to the one of Figure 3B in which the chromophore maintains a nonbonding state immediately after the decay. At the hop the larger positive change in HOOP value would prompt the isomerization to the *E* isomer (i.e., the HOOP value is increasing). However, at this point the wave function is nonbonding (the charge distribution is consistent with an S_0 wave function). The bonding state is reached 10 fs after the hop and in a situation where the HOOP and the C10−C11−C12−C13 are at a turning point. However, the HOOP change appears more rapid and prompts formation of the *Z* isomer consistently with diagram I in Figure 9.

CONCLUSIONS

In recent work,[72] Weingart has analyzed the results of different sets of gas-phase semiclassical CASSCF trajectories for the minimal retinal chromophore model 3-*cis* penta-3,5-dieniminum cation. It has been shown that a general behavior holds for all trajectories: when the S_1 decay occurs during an increase of the H−C3−C4−H dihedral, a 3-*trans* product is formed while when the decay occurs during a decrease of the H−C3−C4−H dihedral the chromophore returns to the original 3-*cis* configuration. The author concludes that simple rules based on the direction of change of the H−C3−C4−H dihedral at the first minimum of the energy difference between S_1 and S_0 can be used to predict the isomerization stereochemistry. The data reported above using suitable QM/MM models of the full Rh and bathoRh systems confirm but also clarify the validity of such rules in terms of electronic effects controlling the stereochemical decision (i.e., the *E*/*Z* branching) taken after the S_1 decay. In particular, the data demonstrate that a HOOP phase control operates (i) after the change of the chromophore bonding status (i.e., of its electronic structure) which is effectively controlled by the BLA mode and (ii) when the change of the C10−C11−C12−C13 dihedral is slow with respect to the amplitude of the HOOP change. As shown for Rh, the change in bonding may not occur upon decay as assumed in previous studies but occurs whenever the BLA mode oscillates toward a FC-S_0-like bonding pattern. Also, as shown in Figure 9C, there may be trajectories where the HOOP rules does not hold due to the limited amplitude of the mode (i.e., condition ii above is not obeyed) relative to the isomerization mode.

The bathoRh and Rh semiclassical trajectories discussed above point to a photochromic cycle mechanism completely consistent with the simple mechanistic diagram of Scheme 1. The potential energy surface schemes of Figures 10A and 10B provide a basis for the interpretation of the trajectory data. After photoexcitation bathoRh travels along an S_1 channel placed ca. 10 kcal mol^{-1} above the S_0 energy surface and it is funneled, immediately after decay at the intersection, along an S_0 exit channel lying below the S_1 energy surface and featuring a diradical (FC-S_0-like) wave function. In contrast, the entry channel that drives the S_1 relaxation of Rh is well separated from S_0. However, the corresponding exit channel has a small S_1−S_0 gap and is initially dominated by a charge transfer (FC-S_1-like) wave function. The opposite progressions of bathoRh and Rh suggest that their reaction coordinates describe opposite space-saving deformations. In fact, Figures 3C and 3D shows fully inverted retinal chromophore motion ultimately involving torsional deformations along the C13−C14, C11−C12 and C9−C10 bonds. As shown by the 59 and 104 fs structures in Figures 10A and 10B, this motion ultimately corresponds to a bicycle-pedal or an asynchronous crankshaft counterclockwise−clockwise−counterclockwise motion in bathoRh and to a clockwise−counterclockwise−clockwise motion in Rh.

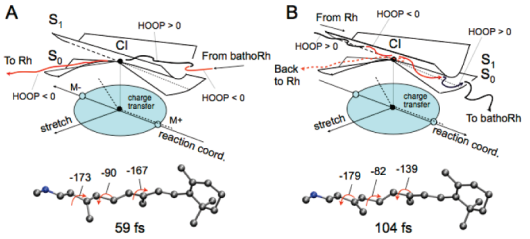

Figure 10. Schematic structure of the S_1 and S_0 potential energy surfaces in the −90° conical intersection region for the systems under investigation. A. Schematic trajectory for bathoRh. B. Schematic trajectories for Rh (full line) and unreactRh (dashed line, see below). The molecular structures at the bottom correspond to the decay (hop) point in the vicinity of the CI. The corresponding geometrical parameters are given in degrees.

In bathoRh and Rh the decay to S_0 and the "chemical" event corresponding to the change from an antibonding to a bonding character of the wave function occur with different points in time. In bathoRh these two events take place simultaneously. As shown in Figure 3E, at the hop the lengths of the N−C15 and C14−C13 bonds are quickly contracting while the C15−C14 bond length is expanding. This BLA phase prompts a bonding (FC-S_0-like diradical) character so that 20 fs after the hop the C11−C12 π-bond reconstitution has started (see Figure 6A). Indeed, the "stereochemical" event deciding between the evolution toward a *Z* or *E* stereoisomer is taken in the same time frame and, as described in Figure 5, is controlled by the phase and sign of the HOOP mode.

The data above indicate that the interplay between the initial value and number of oscillations of the BLA, HOOP and isomerization modes may highly impact the quantum yield of the reaction. In Figure 3C we show that, for bathoRh, the HOOP mode starts at a maximum (positive phase) and performs one full oscillation before decaying at value near 0°. As a consequence, when bond reconstitution begins (triggered by the change in the wave function at the decay point) the HOOP value is rapidly decreasing to −80° prompting formation of a *Z* isomer. This mechanism suggests that a HOOP phase inversion (e.g., as a result of a delay or acceleration of half a period) would change the reaction stereochemical outcome (consistently with the results of ref 72). Notice that the stereochemical outcome also makes the difference between ultrafast photoproduct formation and ultrafast internal conversion.

In Rh the evolution of the HOOP mode is such that the motion starts at an oscillation minimum and, therefore, it is half a period delayed with respect to bathoRh. The HOOP mode oscillates two and a half times before decay and therefore reaches the S_0 state immediately after an oscillation maximum. In this situation one would expect a decrease in the HOOP value that becomes negative and prompts internal conversion (via an aborted isomerization back to the original *Z* stereoisomer). However, the fact that after the decay Rh conserves a FC-S_1-like wave function for ca. 20 fs allows for half HOOP oscillation to be completed before the electronic structure starts to become suitable for double bond reconstitution (i.e., before exiting the dashed area of Figure 7B). This electronic structure is controlled by the phase of the BLA mode. In fact, as is apparent from the inspection of Figure 3F, at the hop the lengths of the N−C15 and

dx.doi.org/10.1021/ja1056196 |*J. Am. Chem. Soc.* 2011, 133, 3354–3364

C14−C13 bonds are quickly expanding while the C15−C14 bond length is contracting. This BLA mode phase prompts an antibonding (charge transfer) character that prevents the C11−C12 π-bond reconstitution. However, 20−25 fs after the decay the BLA mode allows for a bonding situation. At this time the HOOP mode has performed almost three oscillations and it is rapidly growing toward positive values. Ultimately this leads to the formation of the *E* bond. Such a mechanism holds when the C10−C11−C12−C13 dihedral (i.e., the isomerization mode) change is slow with respect to the change in the HOOP value. However, there are situations (e.g., see Figure 9C) in which this is not the case and the amplitude of the HOOP mode plays an important role.

In conclusion, it appears that the phase and amplitude of the HOOP mode, taken at the moment of the change of the wave function character (controlled by the phase of the BLA mode) from charge transfer to diradical, represents a critical event for the control of the stereoselectivity of the photoisomerization of protonated Schiff bases. The trajectories investigated above are released without initial kinetic energy, therefore the described interplay is a mere consequence of the structure of the excited state force field. Namely, the direction of initial mode deformations, amplitudes and phases are imposed by the slope of the potential energy surface. While nonzero initial velocities may result in a different trajectory, decay point and reaction outcome, the stereochemical "rules" based on the overlap relationships of Figures 4, 5 and 9 shall remain valid. The protein environment may exploit this mechanism to enhance the isomerization efficiency in different ways. For instance it could bias the initial S_1 relaxation out of the FC point to either a positive or negative HOOP phase. Alternatively, it could delay the time of the decay to S_0 (i.e., via longer S_1 paths) or, as for Rh, it may use a more complex strategy by conserving the reacting chromophore in the S_1 electronic structure (unfavorable to bond reconstitution) for the time necessary to achieve a favorable HOOP phase. Notice that also the amplitude of the BLA and HOOP oscillation can affect the ratio between successful and unsuccessful events. A lower or higher amplitude shall change the dynamics at the point of decay and during the initial evolution on the S_0 energy surface owing to the fact that in these regions the motion is highly anharmonic. The protein environment may also regulate the amplitude of the HOOP mode in such a way as to favor, rather than disfavor, a rapid evolution toward the photoproduct. We believe that these observations open interesting perspectives for the control of the isomerization stereochemistry and, ultimately, for the understanding of the factors controlling the reaction quantum yield.

■ ASSOCIATED CONTENT

Supporting Information. Details of the trajectory computations. One table with the energies and electronic properties for the bathoRh and Rh equilibrium structures. Cartesian coordinates of the chromophores of bathoRh and Rh equilibrium structures and of the corresponding conical intersections. Cartesian coordinates of the chromophores of the Rh structures of Figure 9. Three movies displaying the change in π-electron density for Rh, bathoRh and unreactRh along the corresponding trajectories. Complete ref 36. This material is available free of charge via the Internet at http://pubs.acs.org.

■ AUTHOR INFORMATION

Corresponding Author
molivuc@bgnet.bgsu.edu

■ ACKNOWLEDGMENT

We wish to thank Tadeusz Andruniów for helpful discussion. This work was supported by the Bowling Green State University. M.O. is grateful to the Center for Photochemical Sciences and the School of Arts & Sciences of Bowling Green State University for start-up funds. We are grateful to the Ohio Supercomputer Center for granted computer time. R.L. is grateful to the Swedish Research Council (VR) for financial support. L.M.F. acknowledges financial support from Project CTQ2009-07120 and "Ramón y Cajal" contract of the Spanish MICINN.

■ REFERENCES

(1) Mathies, R. A.; Lugtenburg, J. In *Handbook of Biological Physics*; Stavenga, D. G., Grip, W. J., Pugh, E. N., Eds.; Elsevier Science: 2000; pp 55−90.
(2) Kandori, H.; Schichida, Y.; Yoshizawa, T. *Biochemistry (Moscow)* **2001**, *66*, 1197–1209.
(3) Hurley, J. B.; Ebrey, T. G.; Honig, B.; Ottolenghi, M. *Nature* **1977**, *270*, 540–542.
(4) Spalink, J. D.; Reynolds, A. H.; Rentzepis, P. M.; Sperling, W.; Applebury, M. L. *Proc. Natl. Acad. Sci. U.S.A.* **1983**, *80*, 1887–1891.
(5) Schick, G. A.; Cooper, T. M.; Holloway, R. A.; Murray, L. P.; Birge, R. R. *Biochemistry* **1987**, *26*, 2556–2562.
(6) Palczewski, K. *Annu. Rev. Biochem.* **2006**, *75*, 743–767.
(7) Bridges, C. D. B. *Biochem. J.* **1961**, *79*, 128–134.
(8) Bridges, C. D. B. *Biochem. J.* **1961**, *79*, 135–143.
(9) Reuter, T. *Nature* **1964**, *204*, 784–785.
(10) Frutos, L. M.; Andruniow, T.; Santoro, F.; Ferré, N.; Olivucci, M. *Proc. Natl. Acad. Sci. U.S.A.* **2007**, *104*, 7764–7769.
(11) Strambi, A.; Coto, P. B.; Frutos, L. M.; Ferré, N.; Olivucci, M. *J. Am. Chem. Soc.* **2008**, *130*, 3382–3388.
(12) Warshel, A. *Nature* **1976**, 679–683.
(13) Warshel, A.; Barboy, N. *J. Am. Chem. Soc.* **1982**, *104*, 1469–1476.
(14) Warshel, A.; Chu, Z. T.; Hwang, J.-K. *Chem. Phys.* **1991**, *158*, 303–314.
(15) Polli, D.; Altoè, P.; Weingart, O.; Spillane, K. M.; Manzoni, C.; Brida, D.; Tomasello, G.; Orlandi, G.; Kukura, P.; Mathies, R. A.; Garavelli, M.; Cerullo, G. *Nature* **2010**, *467*, 440–3.
(16) Bernardi, F.; Olivucci, M.; Robb, M. A. *Chem. Soc. Rev.* **1996**, *25*, 321.
(17) Prokhorenko, V. I.; Nagy, A. M.; Waschuk, S. A.; Brown, L. S.; Birge, R. R.; Miller, R. J. *Science* **2006**, *313*, 1257–61.
(18) Prokhorenko, V. I.; Nagy, A. M.; Brown, L. S.; Miller, R. J. D. *Chem. Phys.* **2007**, *341*, 296–309.
(19) Hayashi, S.; Tajkhorshid, E.; Schulten, K. *Biophys. J.* **2009**, *96*, 403–16.
(20) Virshup, A. M.; Punwong, C.; Pogorelov, T. V.; Lindquist, B. A.; Ko, C.; Martinez, T. J. *J. Phys. Chem. B* **2009**, *113*, 3280–3291.
(21) Weingart, O.; Migani, A.; Olivucci, M.; Robb, M. A.; Buss, V.; Hunt, P. *J. Phys. Chem. A* **2004**, *108*, 4685–4693.
(22) Ishida, T.; Nanbu, S.; Nakamura, H. *J. Phys. Chem. A* **2009**, *113*, 4356–4366.
(23) Szymczak, J. J.; Barbatti, M.; Lischka, H. *J. Chem. Theory Comput.* **2008**, *4*, 1189–1199.
(24) Szymczak, J. J.; Barbatti, M.; Lischka, H. *J. Phys. Chem. A* **2009**, *113*, 11907–11918.
(25) Ruckenbauer, M.; Barbatti, M.; Muller, T.; Lischka, H. *J. Phys. Chem. A* **2010**, *114*, 6757–6765.
(26) Andruniów, T.; Ferré, N.; Olivucci, M. *Proc. Natl. Acad. Sci. U.S.A.* **2004**, *101*, 17908–17913.
(27) Wanko, M.; Hoffmann, M.; Strodel, P.; Koslowski, A.; Thiel, W.; Neese, F.; Frauenheim, T.; Elstner, M. *J. Phys. Chem. B* **2005**, *109*, 3606–3615.
(28) Teller, D. C.; Okada, T.; Bencke, C. A.; Palczewski, K.; Stenkamo, R. E. *Biochemistry* **2001**, *40*, 7761–7772.

(29) Verdegem, P. J. E.; Bovee-Geurts, P. H. M.; de Grip, W. J.; Lugtenburg, J.; de Groot, H. J. M. *Biochemistry* **1999**, *38*, 11316–11324.
(30) Coto, P. B.; Strambi, A.; Ferré, N.; Olivucci, M. *Proc. Natl. Acad. Sci. U.S.A.* **2006**, *103*, 17154–17159.
(31) Mathies, R.; Stryer, L. *Proc. Natl. Acad. Sci. U.S.A.* **1976**, *73*, 2169–2173.
(32) Ferré, N.; Olivucci, M. *J. Mol. Struct.* **2003**, *632*, 71–82.
(33) Besler, B. H.; Kenneth, M. M. M.; Kollman, P. A. *J. Comput. Chem.* **1990**, *11*, 431–439.
(34) Okada, T.; Minoru, S.; Bondard, A.; Elstnerf, M.; Entelc, P.; Buss, V. *J. Mol. Biol.* **2004**, *342*, 571–583.
(35) González, C.; Schlegel, H. B. *J. Phys. Chem.* **1990**, *94*, 5523–5527.
(36) Frisch, M. J. et al. *GAUSSIAN03*, Revision B.04; Gaussian, Inc.: Wallingford, CT, 2003.
(37) Aquilante, F.; De Vico, L.; Ferré, N.; Ghigo, G.; Malmqvist, P.-Å.; Neogrády, P.; Pedersen, T. B.; Pitoňňák, M.; Reiher, M.; Roos, B. O.; Serrano-Andrés, L.; Urban, M.; Veryazov, V.; Lindh, R. *J. Comput. Chem.* **2009**, *31*, 224–247.
(38) Ponder, J. W.; Richards, F. M. *J. Comput. Chem.* **1987**, *8*, 1016.
(39) Swope, W. C.; Andersen, H. C.; Berens, P. H.; Wilson, K. R. *J. Chem. Phys.* **1982**, *76*, 637–649.
(40) Blancafort, L.; Ogliaro, F.; Olivucci, M.; Robb, M. A.; Bearpark, M. J.; Sinicropi, A.; Kutateladze, A. In *Computational methods in photochemistry*; CRC Press: Boca Raton, FL, 2005; pp 31−110.
(41) Groenhof, G.; Bouxin-Cademartory, M.; Hess, B.; deVisser, S. P.; Berendsen, H. J. C.; Olivucci, M.; Mark, A. E.; Robb, M. A. *J. Am. Chem. Soc.* **2004**, *126*, 4228–4233.
(42) Groenhof, G.; Schäfer, L. V.; Boggio-Pasqua, M.; Goette, M.; Grubmüller, H.; Robb, M. A. *J. Am. Chem. Soc.* **2007**, *129*, 6812–6819.
(43) Groenhof, G.; Schäfer, L. V.; Boggio-Pasqua, M.; Grubmüller, H.; Robb, M. A. *J. Am. Chem. Soc.* **2008**, *130*, 3250–3251.
(44) Schäfer, L. V.; Groenhof, G.; Boggio-Pasqua, M.; Robb, M. A.; Grubmüller, H. *PLoS Comput. Biol.* **2008**, *4e*, 1000034.
(45) Boggio-Pasqua, M.; Robb, M. A.; Groenhof, G. *J. Am. Chem. Soc.* **2009**, *131*, 13580–13581.
(46) Weingart, O.; Schapiro, I.; Buss, V. *J. Mol. Model.* **2006**, *12*, 713–721.
(47) Weingart, O.; Schapiro, I.; Buss, V. *J. Phys. Chem. B* **2007**, *111*, 3782–3788.
(48) Groenhof, G.; Boggio-Pasqua, M.; Schäfer, L. V.; Robb, M. A. In *Combining quantum mechanics and molecular mechanics. Some recent progresses in QM/MM methods*; Canuto, S., Sabin, J. R., Eds.; Academic Press: 2010; pp 181−212.
(49) Schapiro, I.; Weingart, O.; Buss, V. *J. Am. Chem. Soc.* **2009**, *131*, 16–17.
(50) Worth, G. A.; Robb, M. A.; Lasorne, B. *Mol. Phys.* **2008**, *106*, 2077–2091.
(51) Hack, M. D.; Wensmann, A. M.; Truhlar, D. G.; Ben-Nun, M.; Martínez, T. J. *J. Chem. Phys.* **2001**, *115*, 1172–1186.
(52) Pan, D.; Ganim, Z.; Kim, J. E.; Verhoeven, M. A.; Lugtenburg, J.; Mathies, R. A. *J. Am. Chem. Soc.* **2002**, *124*, 4857–4864.
(53) Nakamichi, H.; Okada, T. *Angew. Chem., Int. Ed.* **2006**, *45*, 4270–4273.
(54) Nakamichi, H.; Okada, T. *Proc. Natl. Acad. Sci. U.S.A.* **2006**, *103*, 12729–12734.
(55) Eyring, G.; Curry, B.; Broek, A.; Lugtenburg, J.; Mathies, R. *Biochemistry* **1982**, *21*, 384–93.
(56) Loppnow, R. G.; A., M. R. *Biophys. J.* **1988**, *54*, 35–43.
(57) Smith, S. O.; Courtin, J.; de Groot, H.; Gebhard, R.; Lugtenburg, J. *Biochemistry* **1991**, *30*, 7409–7415.
(58) Concistre, M.; Gansmüller, A.; McLean, N.; Johannessen, O. G.; Marin Montesinos, I.; Bovee-Geurts, P. H. M.; Verdegem, P.; Lugtenburg, J.; Brown, R. C. D.; DeGrip, W. J.; Levitt, M. H. *J. Am. Chem. Soc.* **2008**, *130*, 10490–10491.
(59) Gansmüller, A.; Concistrè, M.; McLean, N.; Johannessen, O. G.; Marín-Montesinos, I.; Bovee-Geurts, P. H. M.; Verdegem, P.; Lugtenburg, J.; Brown, R. C. D.; DeGrip, W. J.; Levitt, M. H. *Biochim. Biophys. Acta* **2009**, *1788*, 1350–1357.
(60) Horiuchi, S.; Tokunaga, F.; T, Y. *Biochim. Biophys. Acta* **1980**, *591*, 445–457.
(61) Schreiber, M.; Sugihara, M.; Okada, T.; Buss, V. *Angew. Chem., Int. Ed.* **2006**, *45*, 4274–4277.
(62) Ryde, U.; Nillson, K. *J. Am. Chem. Soc.* **2003**, *125*, 14232–14233.
(63) Kukura, P.; McCamant, D. W.; Yoon, S.; Wandschneider, D. B.; Mathies, R. A. *Science* **2005**, *310*, 1006–1009.
(64) Garavelli, M.; Vreven, T.; Celani, P.; Bernardi, F.; Robb, M. A.; Olivucci, M. *J. Am. Chem. Soc.* **1998**, *120*, 1285–1288.
(65) González Luque, R.; Garavelli, M.; Bernardi, F.; Merchán, M.; Robb, M. A.; Olivucci, M. *Proc. Natl. Acad. Sci. U.S.A.* **2000**, *97*, 9379–9384.
(66) Garavelli, M.; Celani, P.; Bernardi, F.; Robb, M. A.; Olivucci, M. *J. Am. Chem. Soc.* **1997**, *119*, 6891–6901.
(67) Molnar, F.; Ben-Nun, M.; Martínez, T. J.; Schulten, K. *J. Mol. Struct.* **2000**, *506*, 169–178.
(68) Ben-Nun, M.; Molnar, F.; Schulten, K.; Martínez, T. J. *Proc. Natl. Acad. Sci. U.S.A.* **2002**, *99*, 1769–1773.
(69) Martinez, T. J. *Acc. Chem. Res.* **2006**, *39*, 119–126.
(70) Bonačić-Koutecký, V.; Schöffel, K.; Michl, J. *Theor. Chem. Acc.* **1987**, *72*, 459–474.
(71) Bonačić-Koutecký, V.; Koutecký, J.; Michl, J. *Angew. Chem., Int. Ed.* **1987**, *26*, 170–189.
(72) Weingart, O. *Chem. Phys.* **2008**, *349*, 348–355.
(73) Koutecky, J.; Bonačić-Koutecký, V.; Jiří Čížek, J.; Döhnert, D. *Int. J. Quantum Chem.* **1978**, *14* (Suppl. S12), 357–369.
(74) Salem, L. *Acc. Chem. Res.* **1979**, *12*, 87–92.
(75) Coto, P. B.; Strambi, A.; Olivucci, M. *Chem. Phys.* **2008**, *347*, 483–491.

NOTE ADDED IN PROOF

A paper describing the influence of the fast hydrogen motions on the Rh photodynamics has been published after the acceptance of our manuscript (Weingart, O.; Altoè, P.; Stenta, M.; Bottoni, A.; Orlandi, G. and Garavelli, M. *Phys. Chem. Chem. Phys.*, **2011**, in press, DOI: 10.1039/C0CP02496A).